Journal of Molecular Graphics and Modelling 51 (2014) 120–127

Contents lists available at ScienceDirect

Journal of Molecular Graphics and Modelling

journal homepage: www.elsevier.com/locate/JMGM

New *in silico* insights into the inhibition of RNAP II by α-amanitin and the protective effect mediated by effective antidotes

Juliana Garcia[a,*], Alexandra T.P. Carvalho[b], Daniel F.A.R. Dourado[b], Paula Baptista[c], Maria de Lourdes Bastos[a], Félix Carvalho[a,*]

[a] REQUIMTE Laboratory of Toxicology, Department of Biological Sciences, Faculty of Pharmacy, University of Porto, Rua José Viterbo Ferreira n° 228, 4050-313 Porto, Portugal
[b] Department of Cell and Molecular Biology, Computational and Systems Biology, Uppsala University, Biomedical Center Box 596, 751 24 Uppsala, Sweden
[c] CIMO/School of Agriculture, Polytechnic Institute of Bragança, Campus de Santa Apolónia, Apartado 1172, 5301-854 Bragança, Portugal

ARTICLE INFO

Article history:
Accepted 3 May 2014
Available online 14 May 2014

Keywords:
α-Amanitin
Benzylpenicillin
Ceftazidime
Silybin
RNA polymerase II
Trigger loop
Bridge helix

ABSTRACT

Poisonous α-amanitin-containing mushrooms are responsible for the major cases of fatalities after mushroom ingestion. α-Amanitin is known to inhibit the RNA polymerase II (RNAP II), although the underlying mechanisms are not fully understood. Benzylpenicillin, ceftazidime and silybin have been the most frequently used drugs in the management of α-amanitin poisoning, mostly based on empirical rationale. The present study provides an *in silico* insight into the inhibition of RNAP II by α-amanitin and also on the interaction of the antidotes on the active site of this enzyme.

Docking and molecular dynamics (MD) simulations combined with molecular mechanics-generalized Born surface area method (MM-GBSA) were carried out to investigate the binding of α-amanitin and three antidotes benzylpenicillin, ceftazidime and silybin to RNAP II.

Our results reveal that α-amanitin should affects RNAP II transcription by compromising trigger loop (TL) function. The observed direct interactions between α-amanitin and TL residues Leu1081, Asn1082, Thr1083, His1085 and Gly1088 alters the elongation process and thus contribute to the inhibition of RNAP II. We also present evidences that α-amanitin can interact directly with the bridge helix residues Gly819, Gly820 and Glu822, and indirectly with His816 and Phe815. This destabilizes the bridge helix, possibly causing RNAP II activity loss.

We demonstrate that benzylpenicillin, ceftazidime and silybin are able to bind to the same site as α-amanitin, although not replicating the unique α-amanitin binding mode. They establish considerably less intermolecular interactions and the ones existing are essential confine to the bridge helix and adjacent residues. Therefore, the therapeutic effect of these antidotes does not seem to be directly related with binding to RNAP II.

RNAP II α-amanitin binding site can be divided into specific zones with different properties providing a reliable platform for the structure-based drug design of novel antidotes for α-amatoxin poisoning. An ideal drug candidate should be a competitive RNAP II binder that interacts with Arg726, Ile756, Ala759, Gln760 and Gln767, but not with TL and bridge helix residues.

1. Introduction

The poisonous Amanita mushroom species *Amanita phalloides* (Death Cap), *Amanita verna* (White Deadly Amanita) and *Amanita virosa* (Destroying Angel) are responsible for 90–95% of the fatalities occurring after mushroom ingestion [1]. Toxins contained in these species include bicyclic octapeptides and consist of nine defined members: α-amanitin, β-amanitin, γ-amanitin, ε-amanitin, amanin, amanin amide, amanullin, amanullinic acid, and proamanullin [2]. From these, α-amanitin accounts for about 40% of the amatoxins [2].

Specific properties characterize these toxins. They are thermostable and are not removed by boiling and discarding water or by any form of cooking or drying, and belong to the most violent

* Corresponding authors. Tel.: +351 220428597; fax: +351 226093390.
E-mail addresses: jugarcia_18@hotmail.com, garciaju1987@gmail.com (J. Garcia), felixdc@ff.up.pt (F. Carvalho).

http://dx.doi.org/10.1016/j.jmgm.2014.05.002
1093-3263/

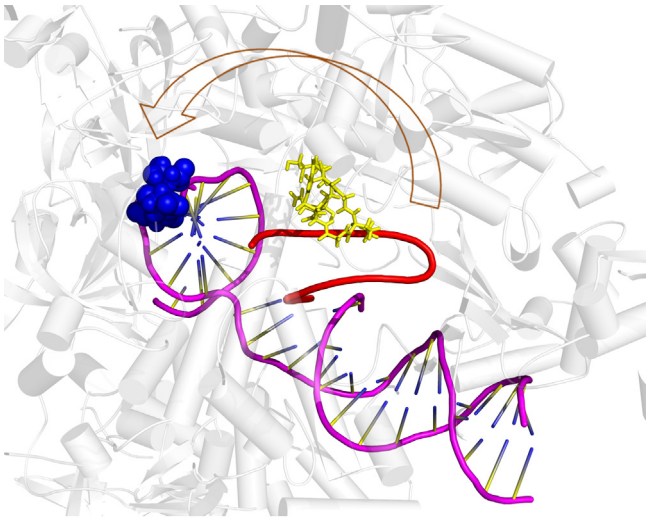

Fig. 1. Structure of RNAP II/α-amanitin complex. Trigger loop, active site, DNA and α-amanitin are colored red, blue, magenta and yellow, respectively. Active site is represented by the Asp 481, Asp 483 and Asp 485 catalytic residues. (For interpretation of the references to color in this figure legend, the reader is referred to the web version of the article.)

poisons from higher fungi: only one medium-size amatoxin-containing specimen contains from 10 to 12 mg amatoxins, a potential lethal dose for human adults (lethal dose: LD_{50} of 0.1–0.5 mg/kg body weight) [3].

After ingestion poisonous Amanita mushrooms, amatoxins are readily absorbed and accumulate in the liver upon uptake *via* an organic anion-transporting octapeptide (OATP) located in the sinusoidal membrane of hepatocytes [4], which is the same transport system for biliary acids. The main molecular mechanism of toxicity is their strong inhibition of RNAP II [5] which is responsible for the transcription of the precursor of messenger RNA. This in turn causes inhibition of DNA and protein synthesis processes and leads to cell death [6].

RNAP II consists of a 10-subunit core enzyme and a peripheral heterodimer of subunits Rpb4 and Rpb7 (Rpb4/7 subcomplex). The core enzyme comprises subunits Rpb1, Rpb2, Rpb3, Rpb5, Rpb6, Rpb8, Rpb9, Rpb10, Rpb11 and Rpb12 [7]. The active site is located in the interface between the core subunits Rpb1 and Rpb2. The catalytic process involves the nucleotide addition cycle (NAC) and begins with binding of a nucleoside triphosphate (NTP) substrate to the elongation complex (EC). Catalytic addition of the nucleotide to the growing 3′-end of the RNA leads to formation of a pyrophosphate ion. Pyrophosphate release leads to the pre-translocation state, in which the newly added, 3′-terminal RNA nucleotide remains in the substrate site. Finally, translocation of DNA and RNA results in the post-translocation state, in which the substrate site is free for binding the next NTP, and the NAC can be repeated [8]. This process involve a structural element named trigger loop (TL), which makes both direct and indirect contact with all features of the nucleotide in the polymerase active center and the bridge helix which guides the template DNA strand in the active site and positions the DNA-RNA hybrid relative to the active site [9]. TL has been hypothesized to have several conformations, but two of them, the "open" (Fig. 1) and "closed" conformations were observed in X-ray structures [9,10]. In the open TL structure the substrate enters on the enzyme, and then the TL rotates (see arrow in Fig. 1) to the active site (closed conformation) [9]. The flexibility of the trigger loop on the catalysis is directly influenced by the conformation of the bridge helix [11]. Recently a crystal structure of α-amanitin with yeast RNAP II was published revealing several key molecular interactions that may contribute to inhibition of RNAP II [10]. Multiple relevant interactions between α-amanitin with RNAP II are located in the bridge helix (previously defined "cleft" region) and in adjacent part of Rpb1 (previously defined funnel region). Based on this α-amanitin may block translocation by interacting with bridge helix and preventing the conformational change of the TL and consequently transcriptional elongation (Fig. 1) [12].

No specific antidote for intoxications with amatoxins is available. Based on pre-clinical findings several antidotes have been used in amatoxin poisonings, including hormones (insulin, growth hormone, glucagon), steroids, vitamin C, vitamin E, cimetidine, thioctic acid, antibiotics (benzylpenicillin, ceftazidime), N-acetylcysteine, and silybin. From these, only benzylpenicillin, ceftazidime, N-acetylcysteine and silybin been reported some success in the pharmacologic management of amatoxin poisonings, though with varying extent [1]. Furthermore, the precise pharmacological mechanism of action for these drugs remains to be elucidated.

In the current study we report the mode of interaction of α-amanitin and three antidotes (benzylpenicillin, ceftazidime and silybin) with RNAP II, using docking methods and molecular dynamics simulations. To secure significant sampling, we performed 3 molecular dynamic simulations (in a total of 34 ns) in explicit water of each one of the RNAP II/α-amanitin/antidotes complexes. In order to provide a new insight into the inhibition mechanism of RNAP II by α-amanitin, and the possible therapeutic mechanism of action of benzylpenicillin, ceftazidime and silybin in amatoxin poisoning, we used binding energy decomposition based on the molecular mechanics generalized Born surface area (MM-GBSA) approach.

2. Materials and methods

2.1. Molecular docking

Molecular Docking of several compounds is helpful in elucidating key features of ligand–receptor interactions. This method allows us to explore the interaction of the antidotes with RNAP II and predict their preferred orientation, which would form a complex with overall minimum energy. The crystal structure of RNAP II complexed with α-amanitin (Protein Data Bank entry 3CQZ and 2VUM) was used to obtain the starting structures for the molecular docking [8,11] and only subunits Rpb1 and Rpb2 were used.

The optimized Rpb1 and Rpb2 subunits were docked with α-amanitin, benzylpenicillin, silybin and ceftazidime. The docking procedure was made with the AutoDock 4 program [13,14]. This automated docking program uses a grid based method for energy calculation of the flexible ligand in complex with a rigid protein. The program performs several runs in each docking experiment. Each run provides one predicted binding mode. The Lamarckian genetic algorithm (LGA) was used in all docking calculations. The $48 \times 44 \times 44$ grid points along the *x*, *y* and *z* axes was centered on the α-amanitin which was large enough to cover all possible rotations of the toxin and antidotes. The distance between two connecting grid points was 0.375 Å. The docking process was performed in 250 LGA runs. The population was 150, the maximum number of generations was 27,000 and the maximum number of energy evaluations was 2.5×106. After complete execution of AutoDock ten conformations of ligand in complex with the receptor were obtained, which were finally ranked on the basis of binding energy [15]. The resulting conformations were visualized in the Visual Molecular Dynamics [16].

After analysis of all the solutions obtained, the best docking solutions were chosen as starting structures for the subsequent minimization and molecular dynamic studies.

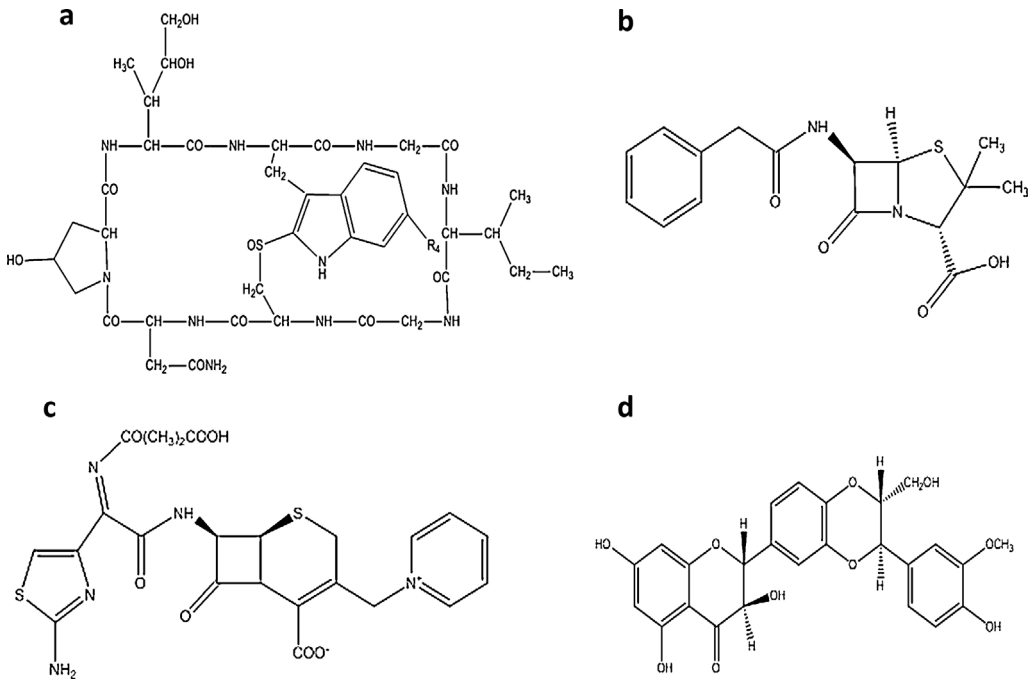

Fig. 2. Chemical structures: (a) α-amanitin; (b) benzylpenicillin; (c) ceftazidime; and (d) silybin.

2.2. Optimization of antidotes and α-amanitin

The structures of α-amanitin, benzylpenicillin, ceftazidime and silybin (Fig. 2) were constructed and optimized in Gaussian at the HF/6-31G* level of theory. For each antidote, we performed two optimizations: one in vacuum and another in the condensed phase. The partial charges were calculated resorting to the RESP method.

2.3. Molecular dynamic simulations

The enzyme was first neutralized by adding Na^+ ions and solvated in a cubic box of TIP3 water molecules, such that there were at least 10.0 Å of water between the surface of the protein and the edge of the simulation box. The initial geometry optimization of the enzyme was minimized in two stages. In the first stage only the hydrogen and water atoms were minimized; in the second stage the entire system was minimized.

The parameters of the chosen models were validated with MD simulations in explicit solvent. The MDs were performed with ff99SB force field and the generalized amber force field (Gaff) [17]. An initial minimization was performed followed by an equilibration of 500 ps. The equilibration was performed in a NVT ensemble using Langevin dynamics with small restraints on the protein (100 kcal mo1^{-1}). For each of the four systems an initial production simulation of 10 ns was performed followed by two random initial velocities replica runs, totaling 34 ns per substrate. This represented a substantial computational effort, since each system is composed by ≈44,000 atoms containing protein, DNA and RNA. Temperature was maintained at 300 K in the NPT ensemble using Langevin dynamics with a collision frequency of 1.0 ps^{-1}. The time step was set to 2 fs. The trajectories were saved every 500 steps for analysis. Constant pressure periodic boundary was used with an average pressure of 1 atm. Isotropic position scaling was used to maintain the pressure with a relaxation time of 2 ps. SHAKE constraints were applied to all bonds involving hydrogen. The particle mesh Ewald (PME) method was used to calculate electrostatic interactions with a cutoff distance of 8.0 Å.

2.4. Calculation of the binding energy

MM-GBSA was applied to compute the binding energy between the protein and each ligand and to decompose the interaction energies on a per residue basis by considering molecular mechanics energies and solvation energies [18].

The energy decomposition was performed for gas-phase energies, desolvation free energies calculated by GB model [19] and nonpolar contributions to desolvation using the linear combinations of pairwise overlaps (LCPO) method [20].

Conformational entropy was not considered because our aim was to identify important interactions between the α-amanitin and the antidotes with RNAP II residues, rather than to obtain very accurate absolute values for the binding free energy.

3. Results and discussion

The determination of the crystal structures with bound α-amanitin it showed that this toxin binding site was quite far from the RNAP II active site. Inhibition could only be explained if α-amanitin binding could lead to some conformational change that would affect the active site. The mystery was partially solved with the determination of the complex RNAP II/DNA.RNA/substrate [9]. In this complex the TL is in the opposite direction and interacting with the substrate. The TL is thus a highly flexible structural motif within the enzyme capable of large conformational changes at each catalytic cycle. Superposition of the pre-catalytic complex with the complex with α-amanitin shows that the large size of the toxin could prevent the movement of the TL (Fig. 3).

Consequently, a description of the full TL movement is still missing. Many TL conformations are still not described and the crystal structures only give initial and final snapshots for this movement. To gain detailed insight about the most important residues for the α-amanitin/antidotes dynamical interaction with RNAP II we performed and analyzed MD simulations on docked complexes of RNAP II/α-amanitin and with the antidotes. Moreover, we performed detailed hydrogen bonds analyses (Table 1), measured the most relevant distances between the protein residues and the

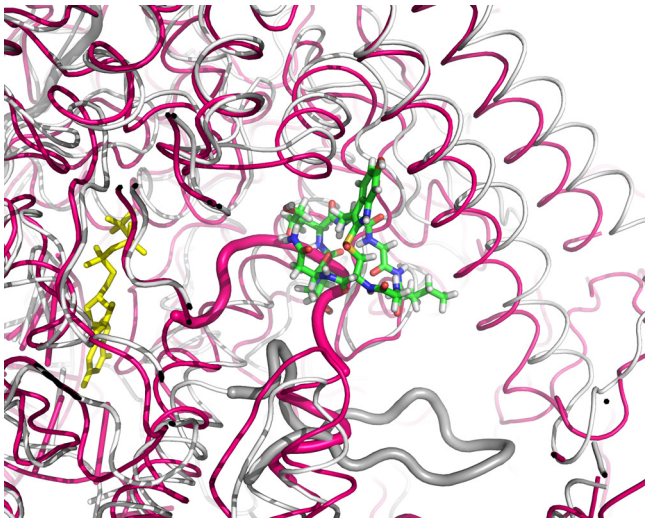

Fig. 3. Interaction of α-amanitin with RNAP II, demonstrated *in silico*. Superposition of the lowest RMSD for the average structure of the simulation (gray), pre-catalytic complex (magenta, pdb code 2E2H), complex with α-amanitin. The α-amanitin is in licorice representation and the substrate is in yellow licorice representation). (For interpretation of the references to color in this figure legend, the reader is referred to the web version of the article.)

toxin/antidotes. Finally, we performed energy decomposition. The protein per residue energy values gives us a fast and relatively reliable estimation of the contribution of each residue to the binding [21]. Our goal was provide a new insight into the inhibition mechanism of RNAP II by α-amanitin by identifying the critical residues for RNAP II binding and subsequently understanding how antidotes interact with RNAP II and if they can bind to the same position without inhibiting the enzyme.

3.1. Identification of critical residues for α-amanitin binding

Superposition of the average simulation structure and the crystal structure is shown in Fig. 4. The most noticeable differences between the crystal structure and our simulation structure rely in the displacement of TL (Fig. 4), which may be attributed to the high flexibility and intrinsic mobility of the TL. In the our simulation structure, Gly1088 residue interacts with α-amanitin oxygen (O33), while in the crystal structure this residue is far away from the α-amanitin. The demonstrated accuracy of the docked complex validates our protocol and supports the results obtained for the antidotes, for which there is no crystal structure (described in Section 3.2).

In order to more easily and accurately grasp the interactions between the protein and α-amanitin we performed an energy decomposition analysis of the simulations. We resorted to the MM-GBSA method. The calculated binding energies of each complex can be seen in Table 2. Even not considering the entropy, computational studies using MM-GBSA calculations on different complexes of protein-inhibitors showed good correlations with respect to experimental data [21]. Individual energy decomposition of all residues in the complex was also calculated in order to qualitatively find the key residues that play a more important role in the α-amanitin binding (Figs. 5a and 6a). Values are expressed as mean ± SD of the 3 replicates. Fig. 5a depicts the relative position of the inhibitor and important residues in the binding complex by using the lowest root-mean-square deviation RMSD structure in respect to the average of the simulation. The toxin α-amanitin interacts with residues Arg726, Ile756, Ala759, Gln760, Gln767, Gln768, Ser769, Gly819, Gly820, Glu822, Leu1081, Asn1082, Thr1083, His1085 and Gly1088 (Figs. 5a and 6a). The guanidinium group of Arg726 forms cation–π interactions with α-amanitin phenyl group, which corresponds to energy of -1.71 ± 1.51 kcal mo1^{-1}. The binding energy of residue Ile756 is -2.53 ± 0.83 kcal mol^{-1}, agreeing with the CH–π interaction of Ile756 alkyl group with α-amanitin phenyl ring. At the same time, Ala759 alkyl group also forms CH–π interactions with α-amanitin phenyl group (-0.67 ± 0.04 kcal mol^{-1}). The side-chain nitrogen atom of Gln760 forms a hydrogen bond with α-amanitin O4 (Table 1), leading to a favorable binding energy of -1.40 ± 0.89 kcal mol^{-1}. Thus the indole portion of α-amanitin inserts in the hydrophobic pocket created by Arg726, Ile756, Ala759 and Gln760 (Fig. 5a). The side-chain oxygen of Gln767 forms a hydrogen bond with α-amanitin N30, which

Table 1
Hydrogen bonds formed between the toxin/antidotes and RNA polymerase II[a].

Toxin/Antidote	Donor	AcceptorH	Acceptor	Distance[b](Å)	Angle[b] (°)	% per time frame
	Gln767:OE1	α-amanitin:H77	α-amanitin:N30	1.81	166.53	60
	α-amanitin:O4	Gln768:HE2	Gln768:NE2	2.87	157.06	80
α-amanitin	α-amanitin:O4	Gln760:HE2	Gln760:NE2	2.11	148.55	26
	α-amanitin:O59	Ser769:H	Ser769:N	2.04	157.88	88
	Glu822:OE1	α-amanitin:1H11	α-amanitin:O63	2.55	172.43	60
Benzylpenicillin	Benzilpenicillin:O3	Hie816:HE2	Hie816:NE2	2.51	134.78	48
	Benzilpenicillin:O1	Gln760:1HE2	Gln760:NE2	1.96	167.45	56
Silybin	Silybin:O56	Gln760:1HE2	Gln760:NE2	2.17	142.68	75
	Silybin:O4	Gly823:H	Gly823:N	2.08	150.30	47

[a] Hydrogen bonds were analyzed in the average structures from MD simulation.

[b] The geometric criterion for the formation of H-bonds is common with an acceptor-donor distance less than 3.5 Å and the donor-H-acceptor angle larger than 120.

Table 2
Binding energy calculation between the three antidotes and α-amanitin with Rpb1 and Rpb2 subunits (all energies are in kcal mol^{-1}).

Complex	ΔG_{ele}	ΔG_{vdw}	ΔG_{Int}	ΔG_{Gas}	ΔG_{GBSUR}	ΔG_{GB}	ΔG_{GBsol}	ΔG_{GBele}	ΔG_{tot}
Rpb1Rpb2/α-amanitin	−60.97	−60.91	0.00	−121.88	−8.16	108.70	100.53	47.73	−21.34
Rpb1Rpb2/benzylpenicillin	−19.78	−31.34	0.00	−51.12	−4.27	41.53	37.26	21.75	−13.87
Rpb1Rpb2/silybin	−21.00	−42.58	0.00	−63.62	−5.87	47.96	42.09	26.95	−21.53
Rpb1Rpb2/ceftazidime	−59.96	−38.20	0.00	−98.16	−5.31	89.94	84.63	29.98	−13.53

ΔG_{ele}: electrostatic energy. ΔG_{vdw}: van der waals energy; ΔG_{int}: internal energy; ΔG_{Gas}: total gas phase energy (sum ΔG_{ele}, ΔG_{vdw}, ΔG_{int}); ΔG_{GBSUR}: nonpolar contribution to solvation; ΔG_{GB}: the electrostatic contribution to the solvation free energy; ΔG_{GBSOL}: sum of nonpolar and polar contributions to solvation; ΔG_{GBELE}: sum of the electrostatic solvation free energy and electrostatic energy; ΔG_{TOT}: estimated total binding energy.

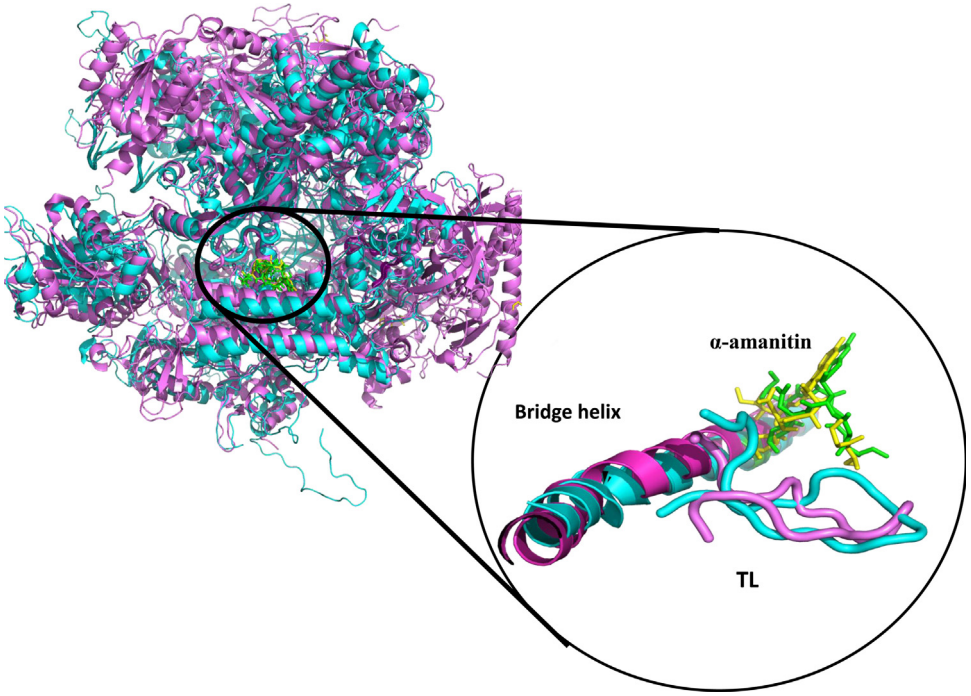

Fig. 4. Superposition of the lowest RMSD for the average structure of RNAP II (cyan) with α-amanitin (green), crystal structure of RNAP II (magenta, pdb code 3CQZ) in complex with α-amanitin (yellow).

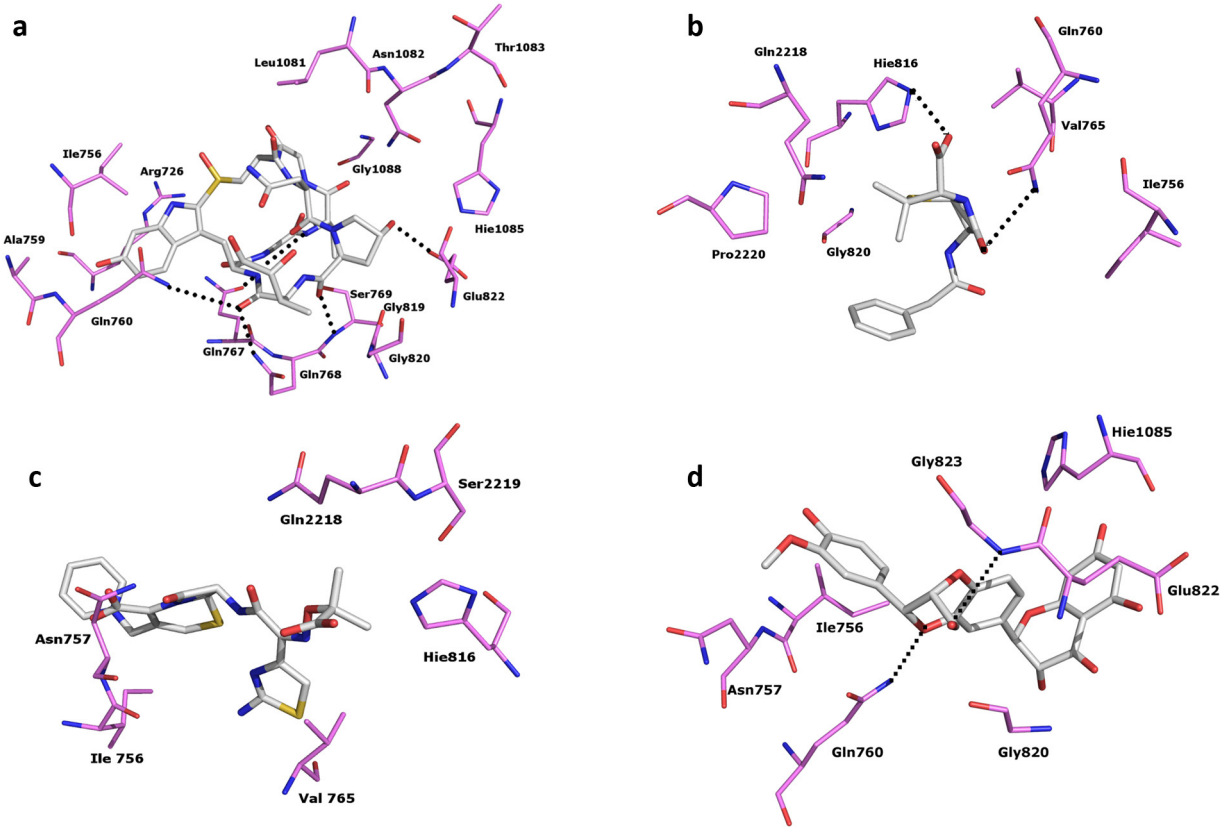

Fig. 5. Geometries of key residues, which produce some favorable interactions with RNAP II, are plotted in the complexes according to the average structure from the MD trajectory. (a) RNAP II/α-amanitin complex; (b) RNAP II/benzylpenicillin complex; (c) RNAP II/ceftazidime complex; and (d) RNAP II/silybin complex. The dashed lines represent hydrogen bonds between the α-amanitin/antidotes and RNAP II.

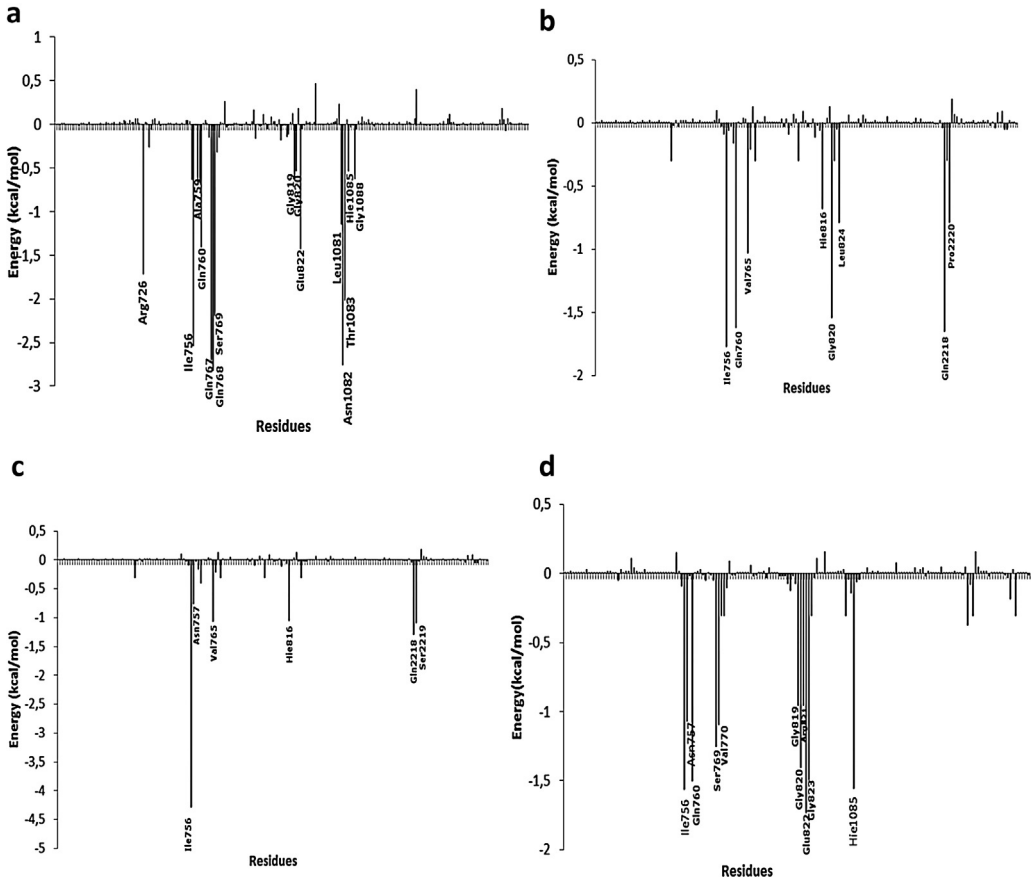

Fig. 6. α-Amanitin/antidotes-residues interaction spectrum of (a) RNAP II/α-amanitin complex; (b) RNAP II/benzylpenicillin complex; (c) RNAP II/ceftazidime complex and (d) RNAP II/silybin complex. The residues with interaction energy than −0.5 kcal mol^{-1} are labeled. Values are expressed as mean ± s.d. of the 3 replicates.

corresponds to interaction energy of −2.70 ± 1.60 kcal mol^{-1}. The nitrogen atom of Gln768 also forms a hydrogen bond with α-amanitin O4 (Table 1), which is the strongest interaction among all residues (−2.82 ± 0.88 kcal mol^{-1}). The α-amanitin/Ser769 interaction energy is −2.18 ± 0.80 kcal mol^{-1}, which is due to a hydrogen bond between Ser769 nitrogen atom and α-amanitin O59 (Table 1). Hydrophobic interactions may be the main force between bridge helix residues Gly819, Gly820 and α-amanitin, which correspond to energies of −0.61 ± 0.08 and −0.53 ± 0.00 kcal mol^{-1}, respectively. The interaction energy of the bridge helix residue Glu822 with α-amanitin is −1.90 ± 0.97 kcal mol^{-1}, corresponding to a hydrogen bond between the Glu822 side chain oxygen and α-amanitin hydroxyproline OH (Table 1). The alkyls group of Leu1081 and Asn1082 interact with α-amanitin alkyls by hydrophobic interactions, which correspond to energies of −1.14 and −2.75 kcal mol^{-1}, respectively. The interaction energy of Thr1083 with α-amanitin is −2.01 kcal mol^{-1}, mostly attributed to dipole–dipole interactions. TL residues His1085 and Gly1088 form dipole–dipole interactions with α-amanitin hydroxyproline and produce interaction energies of −0.53 ± 0.12 and −0.62 kcal mol^{-1}, respectively, which is supporting by experimental data [22].

According to Figs. 5a and 6a and the above analysis, three valuable findings can be observed: (1) Hydrogen bonds, CH–π and hydrophobic interactions drive the bindings of α-amanitin to RNAP II. (2) Our results indicate interactions with bridge helix residues Gly819, Gly820 and Glu822. Moreover, indirect contacts to the bridge helix were also observed. α-Amanitin binds to residue Gln768, which in turn binds to His816 and Phe815 and forms a hydrogen bond with Ser769. Ser769 interacts with the bridge helix residue Gly819. (3) α-Amanitin interacts with TL residues Leu1081, Asn1082, Thr1083, His1085 and Gly1088. These interactions can prevent TL movement and hence contributing to inhibit transcription.

3.2. Binding mode predictions of antidotes to RNAP II

In order to provide a new insight into the mechanism of action of benzylpenicillin, ceftazidime and silybin in amatoxin poisoning we analyzed the antidotes binding to RNAP II.

According to Figs. 5b and 6b, several residues are involved in the RNAP II/benzylpenicillin binding. The binding energy of benzylpenicillin to Ile756 is −1.77 ± 0.49 kcal mol^{-1}, agreeing with CH–π interactions between Ile alkyls and benzylpenicillin phenyl ring (Fig. 5b). Gln760 nitrogen atom binds to benzylpenicillin O1 by a hydrogen bond, corresponding to energy of −1.63 ± 0.45 kcal mol^{-1} (Table 1). At same time, other hydrogen bond between His816 nitrogen and benzylpenicillin O3 contributes with −0.69 ± 0.14 kcal mol^{-1} (Table 1). Val765 alkyl group and benzylpenicillin alkyl group generate dispersive interactions (−1.03 ± 0.14 kcal mol^{-1}). Dipole–dipole interactions are observed between Gly820 and benzylpenicillin (−1.54 ± 0.00 kcal mol^{-1}). Leu824 alkyls groups interact with benzylpenicillin alkyls groups by hydrophobic interactions (−0.79 ± 0.23 kcal mol^{-1}). Finally, Gln2218 and Pro2220 form dipole–dipole interactions with benzylpenicillin carboxyl group, corresponding to energies of −1.65 ± 0.45 and −0.79 ± 0.20 kcal mol^{-1}, respectively. Based on the above analysis, two valuable findings can be described: (1) Residues Ile756, Gln760 and Gly820 are common sites for α-amanitin and benzylpenicillin. (2) Our results indicate that

benzylpenicillin interacts with bridge helix residues His816, Gly820 and Leu824.

In the case of the RNAP II/ceftazidime complex the following residues contribute for binding energy (Figs. 5c and 6c). Ile756 alkyl group and ceftazidime dihydrothiazine ring generate CH–π interactions (Fig. 5c), corresponding to an interaction energy of -4.28 ± 1.70 kcal mol^{-1}. The interaction energy of Asn757 is -0.80 ± 0.10 kcal mol^{-1}, which can be attributed to dipole–dipole interactions with ceftazidime carboxylic acid group. Dipole–dipole interactions between Val765 and ceftazidime propylcarboxy moiety are responsible for energy of -1.06 ± 0.51 kcal mol^{-1}. At same time, identical interactions can be seen between His816 imidazole ring and ceftazidime propylcarboxy moiety (-1.04 ± 0.18 kcal mol^{-1}). Hydrophobic and dipole–dipole interactions are the main forces between Gln2218 and ceftazidime propylcarboxy moiety (-1.30 ± 1.11 kcal mol^{-1}). At same time Ser2219 forms dipole–dipole interactions with the same moiety, which correspond to interaction energy of -1.09 ± 0.38 kcal mol^{-1}. Based on the above analysis, two important conclusions can be obtained: (1) Residue Ile756 and is common site for α-amanitin and ceftazidime. (2) Our results indicate that ceftazidime interact with bridge helix residue His816.

Finally, for RNAP II/silybin binding the key residues are seven (Figs. 5d and 6d). The binding energy of silybin to Ile756 is -1.58 ± 0.27 kcal mol^{-1}, corresponding to a CH–π interaction between Ile756 alkyl and silybin phenyl group. The interaction energy of Asn757 with silybin phenyl ring has energy of -1.06 ± 0.81 kcal mol^{-1}, which mostly results of NH–π interactions. Gln760 side-chain nitrogen forms a hydrogen bond with silybin O56 (-1.50 ± 0.79 kcal mol^{-1}) (Table 1). Dipole–dipole interactions between residues Ser769, Val770, Gly819, Gly820 and Arg821 with silybin result in the energies contributions of -1.25 ± 0.14, -1.01 ± 0.10, 0.95 ± 0.29, -1.40 ± 1.17 and -0.95 ± 0.50 kcal mol^{-1}, respectively. Silybin phenyl ring contacts with Glu822 alkyl group to generate a hydrophobic CH–π interaction (-1.38 ± 0.60 kcal mol^{-1}). The Gly823 forms a hydrogen bond with silybin O4 (-1.49 ± 0.89 kcal mol^{-1}) (Table 1). The π–π contacts and dipole–dipole interactions between residue His1085 and silybin diphenol ring result in an energy contribution of -1.50 ± 0.07 kcal mol^{-1}. From these results, we can conclude: (1) Residues Ile756, Gln760, Gly819, Gly820, Glu822 and His1085 are common sites for α-amanitin and silybin. (2) Our results indicate that silybin interact with bridge helix residues Gly819, Gly820 and Glu822 and TL residue His1085.

4. Conclusions

In this study, docking and MD simulation coupled with MM-GBSA energy decomposition have been carried out to clarify the inhibition mechanism of RNAP II by α-amanitin and to provide a new insight into the plausible mechanism of action of three antidotes used in amatoxin poisoning.

We hypothesize that TL residues Leu1081, Asn1082, Thr1083, His1085 and Gly1088, and bridge helix residues Gly819, Gly820 and Glu822 contribute for the high binding affinity of α-amanitin with RNAP II. Our data clearly reinforces the hypothesis of an important role of the bridge helix [23] and TL in the elongation process and are consistent with the existence of a network of functional interactions between the bridge helix and TL that control fundamental parameters of RNA synthesis. Our data suggest that α-amanitin interferes with bridge helix movement during the translocation and with the movement of the TL, which closes over the active site during the nucleotide incorporation (Fig. 1). Moreover, according to Kaplan et al. (2008), we show that the interaction of α-amanitin with His1085 contributes for the inhibition of the enzyme. This is supported by the findings that a substitution of alanine or phenylalanine at position 1085 specifically renders RNAP II highly resistant to α-amanitin [22]. Also, there are evidences that residue 1085 may play a critical role in the catalytic mechanism [24]. Taken together our results are in good agreement with all literature data.

In the analysis of the antidotes we focused on the TL, bridge helix and other additional residues that are involved in α-amanitin binding. It seems that benzylpenicillin, ceftazidime and silybin, although binding to the same RNAP II binding site, cannot replicate α-amanitin binding mode. The antidotes establish considerably less intermolecular interactions and the ones existing are essential confine to the bridge helix and adjacent residues. The therapeutic effect of the studied antidotes on α-amatoxin poisoning seems not to be directly related with binding to RNAP II.

These structural insights about the molecular aspects of RNAP II inhibition can provide a reliable platform for the structure-based drug design against α-amatoxin poisoning. We suggest that an ideal drug should be a competitive RNAP II binder able to strongly interact with Arg726, Ile756, Ala759, Gln760 and Gln767, but not with bridge helix and TL residues.

Acknowledgements

The authors gratefully acknowledge the Foundation for the Science and Technology (FCT, Portugal) for financial support and also thank FCT for PhD grant SFRH/BD/74979/2010. We acknowledge Qtrex cluster and SNIC-UPPMAX for CPU time allocation.

References

[1] F. Enjalbert, S. Rapior, J. Nouguier-Soule, S. Guillon, N. Amouroux, C. Cabot, Treatment of amatoxin poisoning: 20-year retrospective analysis, J. Toxicol. Clin. Toxicol. 40 (2002) 715–757.
[2] J. Vetter, Toxins of amanita phalloides, Toxicon 36 (1998) 13–24.
[3] T. Wieland, Progress in Tryptophan and Serotonin Research, Walter de Gruyter & Co, Berlin, New York, 1984.
[4] K. Letschert, H. Faulstich, D. Keller, D. Keppler, Molecular characterization and inhibition of amanitin uptake into human hepatocytes, Toxicol. Sci. 91 (2006) 140–149.
[5] T.J. Lindell, F. Weinberg, P.W. Morris, R.G. Roeder, W.J. Rutter, Specific inhibition of nuclear RNAP II by alpha-amanitin, Science 170 (1970) 447–449.
[6] T. Wieland, The toxic peptides from amanita mushrooms, Int. J. Pept. Protein Res. 22 (1983) 257–276.
[7] P. Cramer, K.J. Armache, S. Baumli, S. Benkert, F. Brueckner, C. Buchen, et al., Structure of eukaryotic RNA polymerases, Annu. Rev. Biophys. 37 (2008) 337–352.
[8] F. Brueckner, J. Ortiz, P. Cramer, A movie of the RNA polymerase nucleotide addition cycle, Curr. Opin. Struct. Biol. 19 (2009) 294–299.
[9] D. Wang, D.A. Bushnell, K.D. Westover, C.D. Kaplan, R.D. Kornberg, Structural basis of transcription: role of the trigger loop in substrate specificity and catalysis, Cell 127 (2006) 941–954.
[10] D.A. Bushnell, P. Cramer, R.D. Kornberg, Structural basis of transcription: alpha-amanitin-RNAP II cocrystal at 2.8 A resolution, Proc. Natl. Acad. Sci. U. S. A. 99 (2002) 1218–1222.
[11] L. Tan, S. Wiesler, D. Trzaska, H. Carney, R. Weinzierl, Bridge helix and trigger loop perturbations generate superactive RNA polymerases, J. Biol. 7 (2008) 1–15.
[12] X.Q. Gong, Y.A. Nedialkov, Z.F. Burton, Alpha-amanitin blocks translocation by human RNAP II, J. Biol. Chem. 279 (2004) 27422–27427.
[13] G.M. Morris, D.S. Goodsell, R.S. Halliday, R. Huey, W.E. Hart, R.K. Belew, et al., Automated docking using a Lamarckian genetic algorithm and an empirical binding free energy function, J. Comput. Chem. 19 (1998) 1639–1662.
[14] G.M. Morris, R. Huey, W. Lindstrom, M.F. Sanner, R.K. Belew, D.S. Goodsell, et al., AutoDock4 and AutoDockTools4: automated docking with selective receptor flexibility, J. Comput. Chem. 30 (2009) 2785–2791.
[15] R. Huey, G.M. Morris, A.J. Olson, D.S. Goodsell, A semiempirical free energy force field with charge-based desolvation, J. Comput. Chem. 28 (2007) 1145–1152.
[16] W. Humphrey, A. Dalke, K. Schulten, VMD: visual molecular dynamics, J. Mol. Graph. 14 (1996) 33–38.
[17] D.A. Case, T.E. Cheatham, T. Darden, H. Gohlke, R. Luo, K.M. Merz, et al., The Amber biomolecular simulation programs, J. Comput. Chem. 26 (2005) 1668–1688.
[18] P.A. Kollman, I. Massova, C. Reyes, B. Kuhn, S. Huo, L. Chong, et al., Calculating structures and free energies of complex molecules: combining molecular mechanics and continuum models, Acc. Chem. Res. 33 (2000) 889–897.

[19] A. Onufriev, D. Bashford, D.A. Case, Modification of the generalized born model suitable for macromolecules, J. Phys. Chem. B 104 (2000) 3712–3720.
[20] J. Weiser, P.S. Shenkin, W.C. Still, Approximate atomic surfaces from linear combinations of pairwise overlaps (LCPO), J. Mol. Biol. 20 (1999) 217–230.
[21] P.D. Lyne, M.L. Lamb, J.C. Saeh, Accurate prediction of the relative potencies of members of a series of kinase inhibitors using molecular docking and MM-GBSA scoring, J. Med. Chem. 49 (2006) 4805–4808.
[22] C.D. Kaplan, K.M. Larsson, R.D. Kornberg, The RNAP II trigger loop functions in substrate selection and is directly targeted by alpha-amanitin, Mol. Cell 30 (2008) 547–556.
[23] Y.A. Nedialkov, K. Opron, F. Assaf, I. Artsimovitch, M.L. Kireeva, M. Kashlev, et al., The RNA polymerase bridge helix YFI motif in catalysis, fidelity and translocation, BBA – Gene Regul. Mech. 1829 (2013) 187–198.
[24] A.T.P. Carvalho, P.A. Fernandes, M.J. Ramos, The catalytic mechanism of RNAP II, J. Chem. Theory Comput. 7 (2011) 1177–1188.